Dll1-mediated Notch signaling drives tumor cell crosstalk with cancer associated fibroblasts to promote radioresistance in breast cancer

Ajeya Nandi[1], Rahul Debnath[1], Anupma Nayak[2], Tsun Ki Jerrick To[3], Gatha Thacker[1, 7], Megan Reilly[1], Sanjeev Gumber[4], Ilias Karagounis[5], Ning Li[1], Christopher J. Lengner[1,6], Malay Haldar[3], Alana L. Welm[8], Andres, M Blanco[1,6], Christoforos Thomas[5], Rumela Chakrabarti[1,6, 7*]

[1]Department of Biomedical Sciences, University of Pennsylvania, Philadelphia, PA 19104
[2]Department of Pathology and Laboratory Medicine, Perelman School of Medicine, University of Pennsylvania Philadelphia, Pennsylvania, PA 19104
[3]Department of Pathology and Laboratory Medicine, Perelman School of Medicine, University of Pennsylvania, PA 19104-6160
[4]Department of Pathology and Laboratory Medicine, Emory University, School of Medicine, Atlanta, GA 30329
[5]Department of Radiation Oncology, Perelman School of Medicine, University of Pennsylvania, Philadelphia, PA 19104
[6]Institute for Regenerative Medicine, University of Pennsylvania, Philadelphia, PA 19104
[7]Department of Surgery, Miller School of Medicine, Sylvester Comprehensive Cancer Center, Miami, FL 33136, USA
[8]Department of Oncological Sciences, Huntsman Cancer Institute, University of Utah, Salt Lake City, UT 84112

[*] Corresponding Author

Correspondence to:

Rumela Chakrabarti, PhD

Department of Surgery, Miller School of Medicine

Sylvester Comprehensive Cancer Center

Room 508, Biomedical Research Building

1501 NW 10th Avenue, 5th Floor

Miami, FL 33136

Office phone: 305-243-6545

Cell:3303891943

Email :rxc1335@med.miami.edu

SUPPLEMENTAL FIGURE LEGENDS

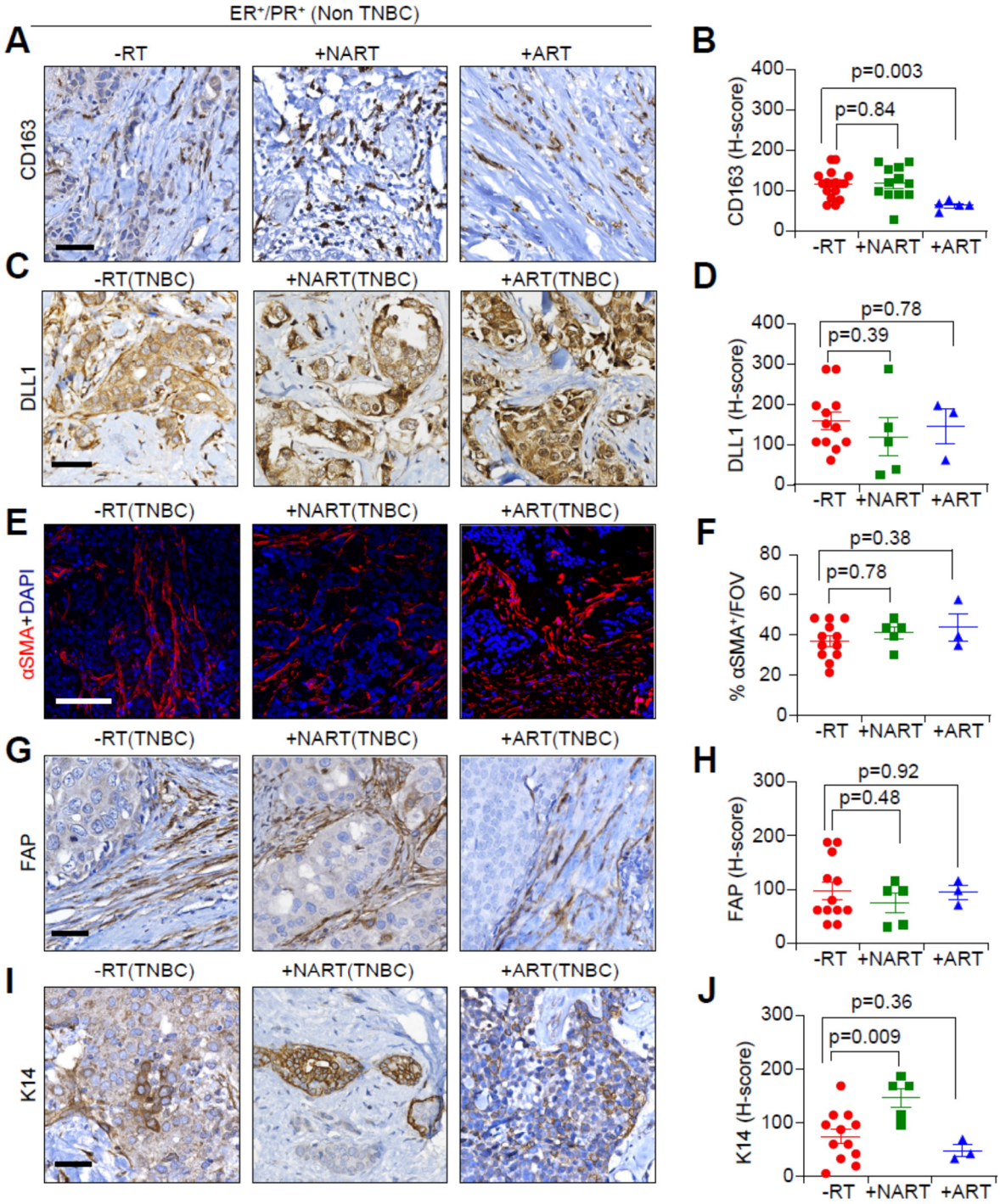

Figure S1. Triple negative breast cancer (TNBC) tumors post radiation does not show increase in DLL1 or FAP expression. (A and **B)** Representative IHC images (**A**) and

quantification of expression of CD163 (**B**), in untreated (-RT), neoadjuvant treated (+NART) and adjuvant treated (+ART) human non-TNBC patient tumors (n=17 tumors from -RT, n=12 tumors from +NART and n=5 +ART tumors. (**C-F**) Representative IHC images and quantification of expression of DLL1 (**C** and **D**) and representative IF images and quantification of expression of αSMA (**E** and **F**) in indicated TNBC patient tumors. (**G-J**) Representative IHC images and quantification of expression of FAP (**G** and **H**) and K14 (**I** and **J**) in indicated TNBC patient tumors (n= 12 tumors for -RT, n=5 +NART and n=3 +ART breast tumors). Each dot in scatter plots represents individual human patient tumors per group. Data are presented as the mean ± SEM. Unpaired student's *t* test was used to calculate p values. FOV stands for field of view. Scale bars, 100 μM.

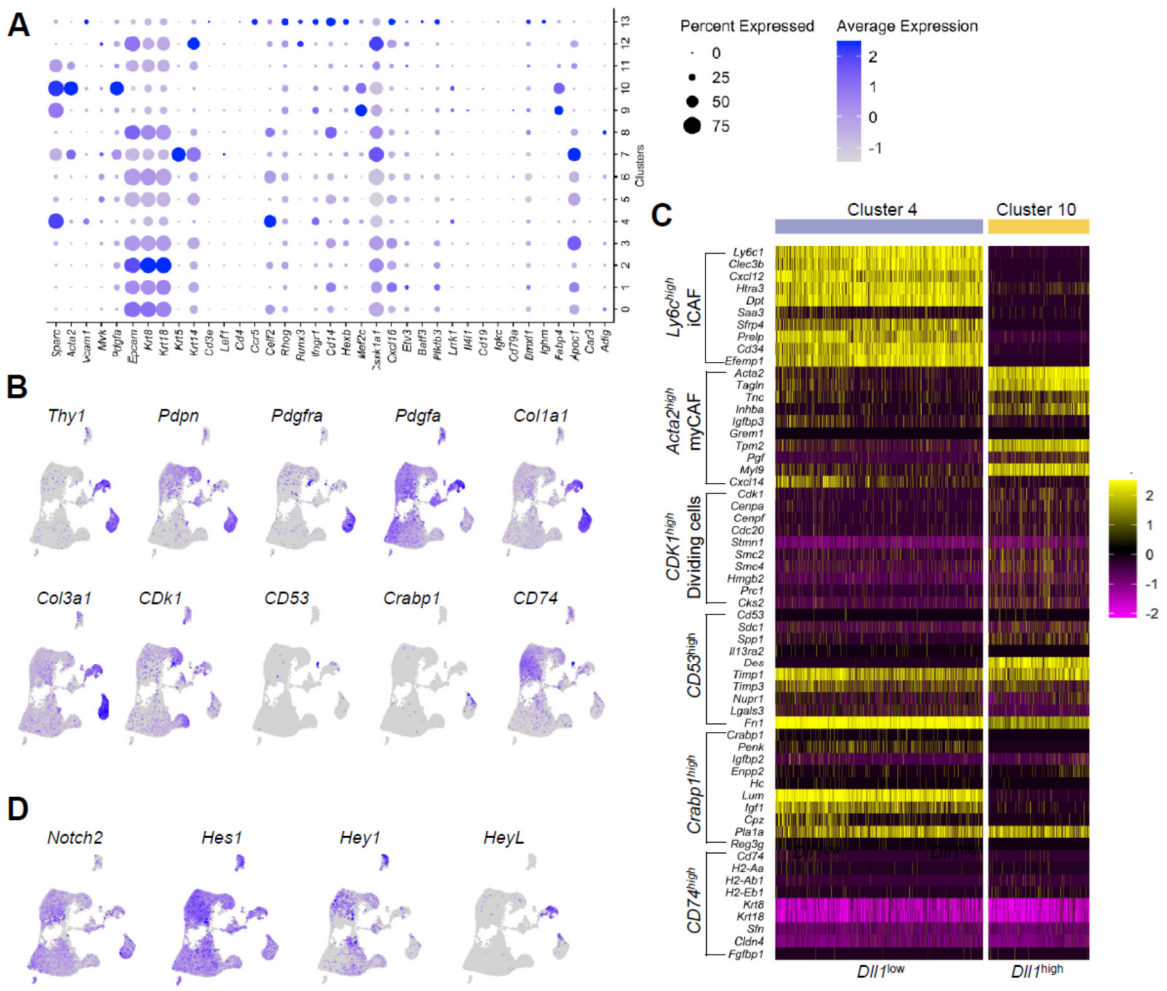

Figure S2. Characterization of CAF subtypes and activation of Notch signaling in MMTV-PyMT luminal breast tumors. (**A**) Feature plots with epithelial markers show epithelial populations are clusters 0-3, 5-8, and 11-12. (**B**) Feature plots show predominant expression of different CAF markers in cluster 4 and 10. (**C**) Heat map depicts a subset of genes differentially expressed in the indicated six CAF subtypes. Legend shows a color gradient of normalized expression. (**D**) Feature plots show the expression of *Notch2* receptor and different Notch signaling target genes (*Hes1*, *Hey1*, *HeyL*) in different clusters from CD45^{-} Dll1^{+} tumor cells.

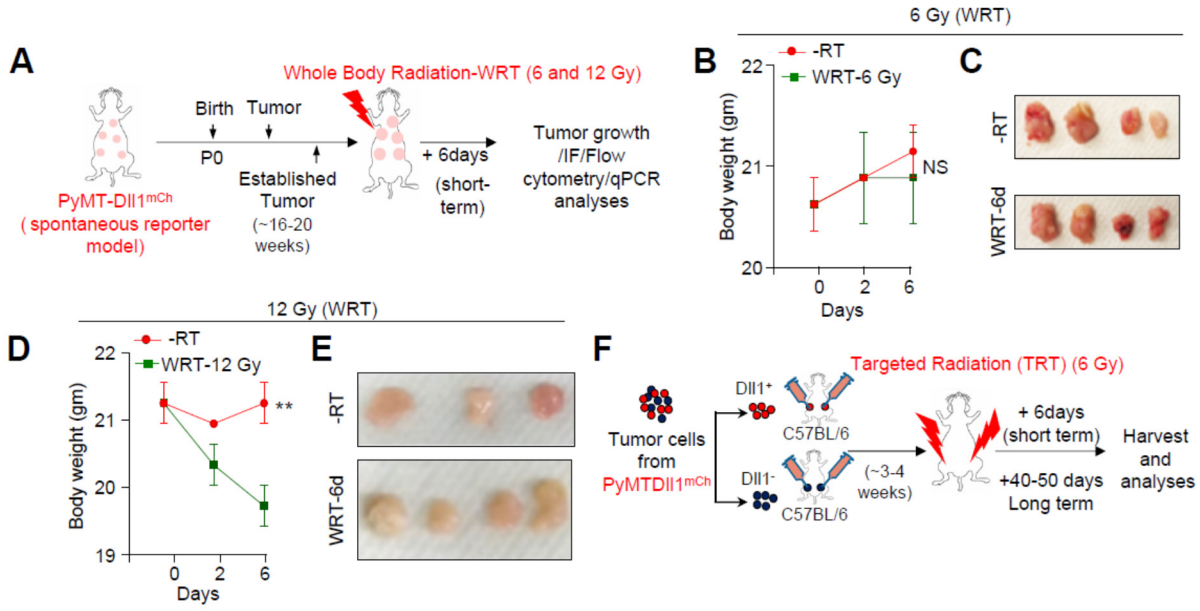

Figure S3. Characterization of different doses of whole-body radiation in MMTV-PyMT Dll1^{mCherry} **murine breast cancer model.** (**A**) Schematic representation of experimental (whole-body radiation, WRT) mouse model where two independent cohorts of spontaneous tumor bearing MMTV-PyMT-Dll1^{mCherry} (Py-Dll1^{mCh}) mice received two doses of whole-body radiation, 6 Gy and 12 Gy respectively. RT was given when tumor sizes were established and after 6 days of radiation (short-term) were sacrificed for analyses (n=3 mice/group), (each mouse had more than one mammary tumor). (**B**) Body weight of mice treated with 6 Gy of WRT did not show any significant difference compared to -RT mice. (**C**) Representative tumor images from -RT and WRT-6 Gy mice. (**D**) Body weight of mice treated with 12 Gy of WRT was significantly reduced compared to -RT mice. (**E**) Representative tumor images from untreated -RT and WRT-12 Gy mice, n=3 mice/group (each mouse had more than one mammary tumor). (**F**) Schematic representation of experimental (targeted radiation-TRT) mouse model. Dll1^{+} and Dll1^{-} tumor cells were sorted from spontaneous Py-Dll1^{mCh} spontaneous tumors and were injected into the mammary fat pad (MFP) of C57BL/6 mice. Single dose of TRT (6Gy) was given when tumors were established. Mice were sacrificed at 6 days (short-term) and 40-50 days (long-term) of radiation and all experiments were performed after that endpoint. Data are presented as the

mean ± SEM. Two-way ANOVA with Bonferroni post-test adjustment (**B** and **D**) was performed to calculate p values. **p < 0.01, NS= not significant.

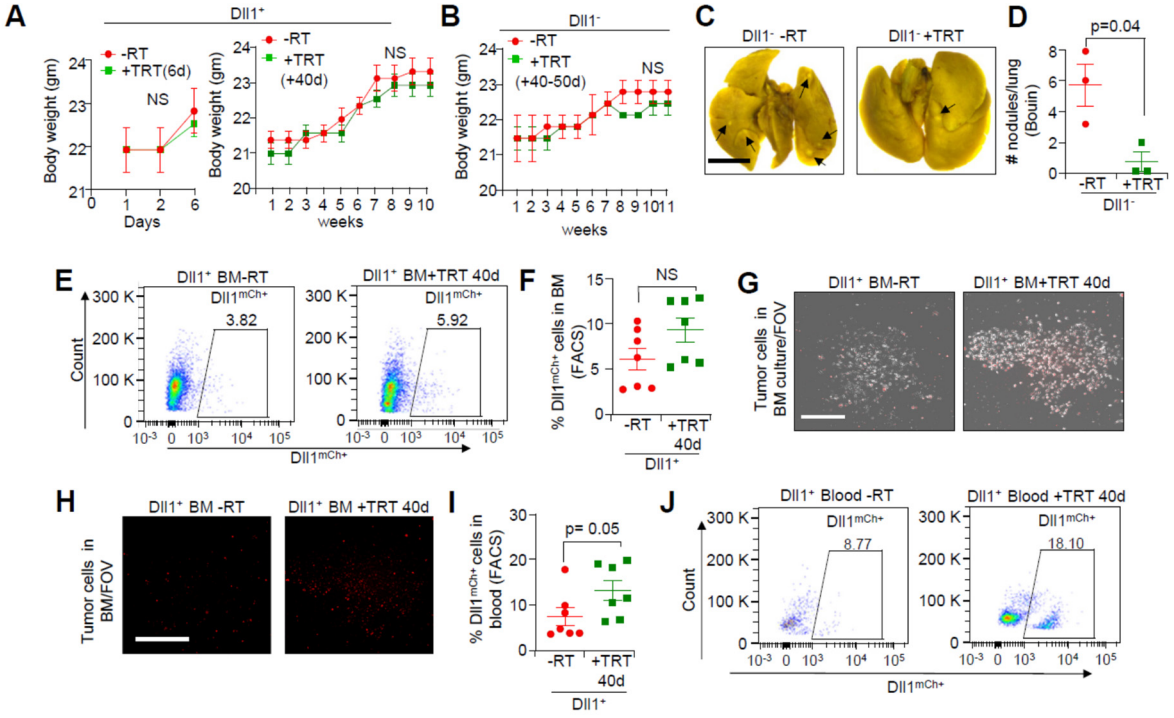

Figure S4. Targeted radiation increases lung and bone metastasis and CTCs (circulating tumor cells) in aggressive breast cancer mouse model. (**A**) Body weight of Dll1^{+} tumor cells implanted mice treated with 6 Gy of short-term (left panel) and long-term (right panel) targeted radiation did not show any significant difference compared to non-irradiated mice. (**B**) Body weight of Dll1^{-} tumor cells implanted mice treated with 6 Gy of long-term targeted radiation shows no alteration compared to non-irradiated mice. (**C** and **D**) The representative whole mount lung images and scatter plot showing fewer number of metastatic lung nodules (black arrows) in Dll1^{-} lung after targeted radiation. The lung nodules were quantified under dissection microscope after 24 hours fixation with Bouin's solution (n=3 lungs/group). (**E**) Flowcytometry analysis shows higher percentage of Dll1^{mCh+} cells in +TRT bone marrow (BM) than -RT bone marrow. (**F**) Scatter plot represents quantification from (**E**). (**G** and **H**) Phase contrast and fluorescence images show number of infiltrated Dll1^{mCh+} tumor cells (red) after 7 days *ex vivo* culture of bone marrow cells.

(**I**) Flowcytometry analysis show higher percentage of disseminated Dll1^{mCh+} cells in blood (CTCs) post targeted radiation. Data was combined from two independent experiments. (**J**) Representative FACS plots from (**I**). Data are presented as the mean ± SEM. Two-way ANOVA with Bonferroni post-test adjustment was performed to calculate p values (**A** and **B**). NS=not significant. Unpaired student's *t* test was used to calculate p values (**D, F** and **I**). Scale bars: 4mm (**C**) and 500 µm (**G** and **H**). FOV =field of view

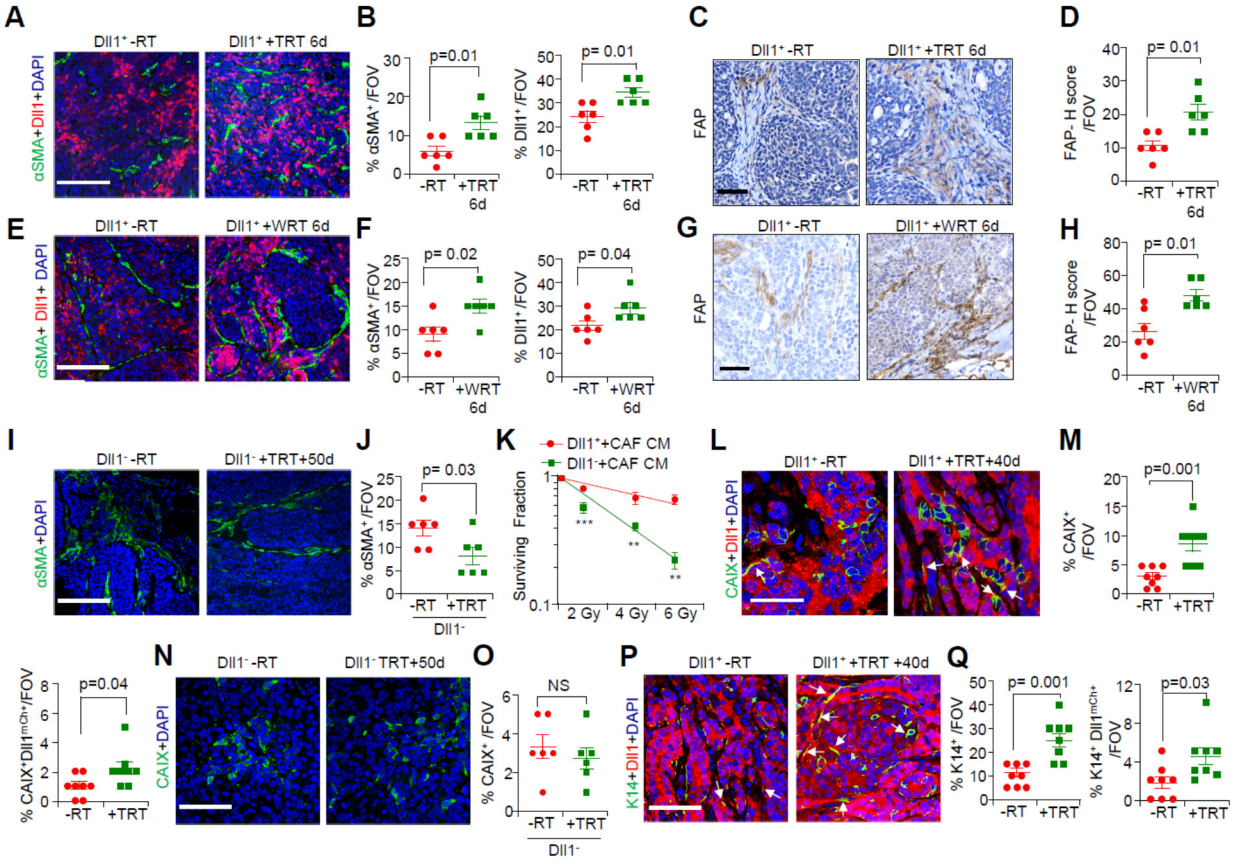

Figure S5. αSMA⁺ CAF infiltration is higher in irradiated Dll1⁺ primary tumors in contrast to non-irradiated Dll1⁺ and Dll1⁻ primary tumors and is associated with increase in hypoxia and K14 expression. (**A** and **B**) Representative IF images (**A**) and quantification (**B**) showing higher expression of αSMA⁺ CAFs and Dll1⁺ tumor cells in +TRT Dll1⁺ tumors compared to -RT Dll1⁺ tumors post short term targeted radiation (TRT 6d). (**C** and **D**) Representative IHC images (**C**) and quantification (**D**) showing higher expression of FAP⁺ cells in +TRT Dll1⁺ tumors compared to -RT Dll1⁺ tumors post short term targeted radiation (TRT 6d). (**E** and **F**) Representative IF images (**E**) and quantification (**F**) represent increased expression of αSMA⁺ CAFs and Dll1⁺ tumor cells in +WRT 6d Dll1⁺ tumors compared to -RT Dll1⁺ tumors. (**G** and **H**) Representative IHC images (**G**) and quantification (**H**) represent increased expression of FAP⁺ cells in +WRT 6d Dll1⁺ tumors compared to -RT Dll1⁺ tumors. (**I** and **J**) Representative IF images (**I**) and quantification (**J**) showing decreased αSMA⁺ cells in +TRT Dll1⁻ primary tumors compared

to -RT Dll1^{-} primary tumors. (**K**) Clonogenic survival assay graph showing greater percentage of survival fraction of Dll1^{+} tumor cells than Dll1^{-} tumor cells when cultured with Py-Dll1^{WT} CAF condition medium (CM) post radiation. (**L** and **M**) Representative IF images (**L**) and quantification (**M**) show increased number of hypoxic CAIX^{+} tumor cells and the co-localization of Dll1^{mCh+} and CAIX^{+} tumor cells in +TRT Dll1^{+} primary tumor compared to -RT Dll1^{+} primary tumor. (**N** and **O**) Representative IF images (**N**), and quantification (**O**) show decreased CAIX^{+} cells in +TRT Dll1^{-} primary tumors compared to -RT Dll1^{-} primary tumors. (**P** and **Q**) Representative IF images (**P**) and quantification (**Q**) show increased number of K14^{+} tumor cells and the co-localization of Dll1^{mCh+} and K14^{+} cells in +TRT Dll1^{+} primary tumors compared to -RT Dll1^{+} primary tumors. White arrowheads indicate double positive staining. The dots in each scatter plot represent the field of views (FOVs), which is obtained from n=6 tumors/group. Data are presented as the mean ± SEM. Unpaired student's *t* test was used calculate p values. **$p < 0.01$, ***$p < 0.001$. Scale bars, 100 μm. NS= not significant.

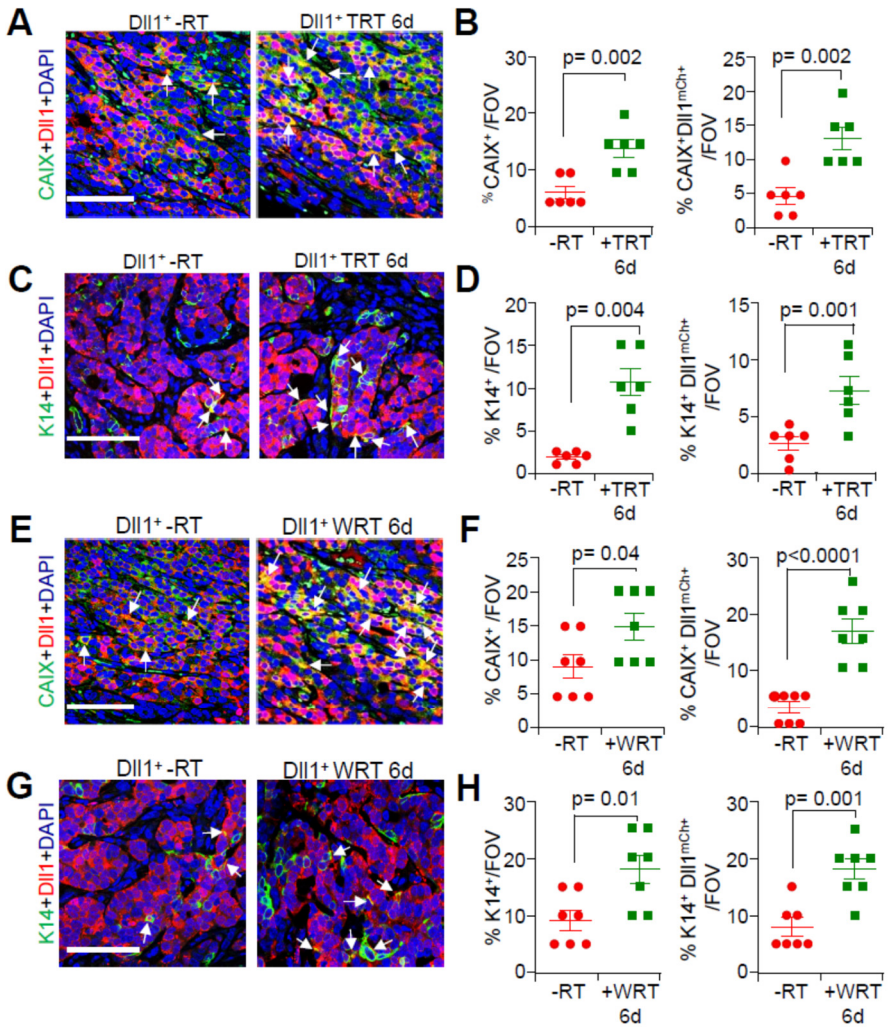

Figure S6. Short-term targeted and whole-body radiation increases hypoxic Dll1⁺ tumor cells and K14⁺ Dll1⁺ double positive tumor cells in primary breast tumors. (**A-D**) Representative immunofluorescence (IF) images (**A**) and quantification (**B**) show increased positive cells for a hypoxic marker, CAIX and the co-localization of Dll1 and CAIX positive cells and representative IF images (**C**) and quantification (**D**) show increased a basal/stem-like cell marker, K14 and the co-localization of Dll1 and K14 positive cells in +TRT 6d Dll1⁺ primary breast tumors compared to -RT Dll1⁺ primary breast tumors. (**E-H**) Representative IF images (**E**) and quantification (**F**) show increased positive cells for a hypoxic marker, CAIX and the co-localization of Dll1 and CAIX positive cells and representative IF images (**G**) and quantification (**H**) a basal

stem cell marker, K14 and the co-localization of Dll1 and K14 positive cells in +WRT 6d Dll1^{+} primary breast tumors compared to -RT Dll1^{+} primary breast tumors. White arrowheads indicate double positive staining. The dots in each scatter plot represent the field of views (FOVs), which is obtained from n= 6 tumors/group. Data are presented as the mean ± SEM. Unpaired student's *t* test was used to calculate p values. Scale bars, 100 μm.

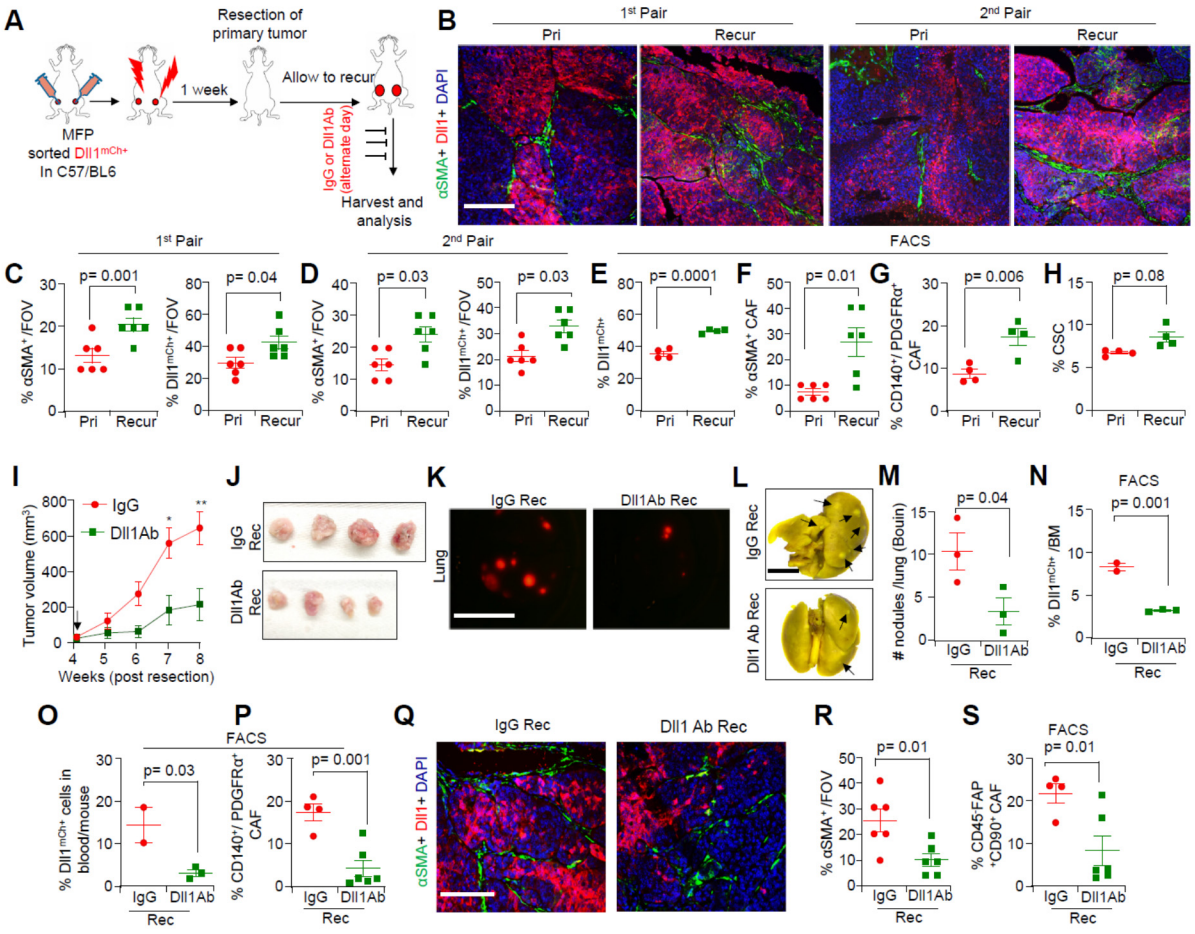

Figure S7. **Recurred tumors post radiation and resection show an increase CSC and αSMA⁺ CAF populations after TRT and pharmacological inhibition of Dll1 can sensitize these recurrent PyMT-Dll1⁺ tumors to radiotherapy.** (**A**) Schematic representation showing the experimental plan of resection of Dll1⁺ primary tumors and *in vivo* anti-Dll1-blocking antibody treatment. (**B-D**) Representative immunofluorescence (IF) images (**B**), scatter plot quantification (**C** and **D**) showing increased αSMA⁺ CAFs and of Dll1⁺ tumor cells in two pairs (out of 3 pairs) of recurrent Dll1⁺ tumors compared with matched resected Dll1⁺ tumors after TRT. (**E-H**) Flowcytometry graphs showing a greater number of Dll1⁺ tumor cells (**E**), αSMA⁺ myCAFs (**F**), CD140⁺/PDGFRα⁺ CAFs (**G**) and CSCs (CD24⁻CD44⁺) (**H**) in recurrent Dll1⁺ tumors compared to their matched resected Dll1⁺ tumors (For **E, G** and **H** n=4 tumors/group and for **F** n=6 tumors/group). (**I** and **J**) Tumor progression graph (**I**) and representative whole tumor images (**J**)

showing decreased tumor growth in recurrent Dll1^{+} tumors after treated with anti-Dll1 antibody compared to IgG control tumors (n=6 tumors/group). Black arrow defines start time of treatment (2 days post RT). (**K-M**) Representative dissecting FL and bright field images of whole mount lung images (**K** and **L**), and scatter plots (**M**) showing fewer metastatic nodules upon anti-Dll1 antibody treatment (n=3 mice/group). (**N-P**) Flowcytometry analyses in scatter plots showing reduced number of Dll1^{mCh+} cells in bone marrow (BM) blood (**N** and **O**), CD140^{+}/PDGFRα^{+} CAFs (**P**) upon anti-Dll1-blocking antibody treatment in mice compared to IgG treated mice. (**Q** and **R**) Representative IF images (**Q**) and scatter plot (**R**) showing decreased number of αSMA^{+} expressing CAFs in recurrent tumor after anti-Dll1-blocking antibody treatment compared to IgG treatment. The dots in scatter plot represent the field of views (FOVs), obtained from n=4 tumors/group. (**S**) Flowcytometry analyses in scatter plots showing decreased number of CD45^{-} FAP^{+}CD90^{+} CAFs in recurrent tumors upon *in vivo* Dll1 blocking compared to IgG treated tumors. Data are presented as the mean ± SEM. Two-way ANOVA with Bonferroni post-test (**I**), Paired Student's *t* test (**C-H**) and unpaired student's *t* test (**M-P, R** and **S**) were used to calculate p values. *p < 0.05; ** p<0.01. Scale bars, 100 μm (**B** and **Q**) and 4mm (**K** and **L**).

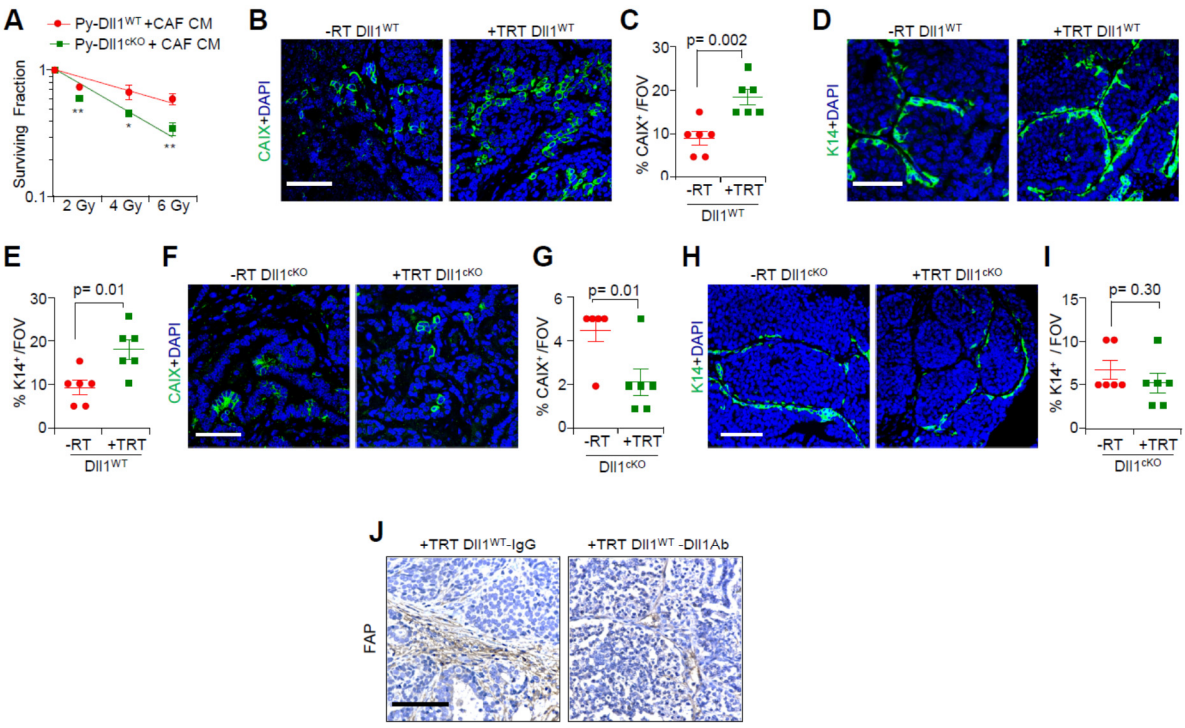

Figure S8. Loss of Dll1 decreases hypoxia and K14⁺ tumor cells in primary breast tumors upon long term targeted radiation. (**A**) Clonogenic survival assay graph showing greater percentage of survival fraction of Py-Dll1^{WT} tumor cells than Py-Dll1^{cKO} tumor cells when cultured with Py-Dll1^{WT} CAF condition medium (CM) after radiation. (**B-E**) Representative immunofluorescence (IF) confocal images and quantification show a greater number of CAIX⁺ hypoxic tumor cells (**B** and **C**) and K14⁺ tumor cells (**D** and **E**) in +TRT Py-Dll1^{WT} tumors compared to -RT Py-Dll1^{WT} tumors. (**F-I**) Representative IF images and quantification showing dramatic decrease in CAIX⁺ hypoxic tumor cells (**F** and **G**) and slight decrease in K14⁺ tumor cells (**H** and **I**) in +TRT Py-Dll1^{cKO} tumors compared to -RT Py-Dll1^{cKO} tumors. The dots in each scatter plot represent field of views (FOVs), which is obtained from n=6 tumors/group. (**J**) Representative IHC image showing decrease in FAP⁺ CAFs in +TRT Py-Dll1^{WT} tumors after Dll1 Ab treatment compared to IgG treatment. Please refer to **Fig. 4T** for quantification. Data are presented as the

mean ± SEM. Unpaired student's *t* test was used (**A**, **C**, **G**, **E** and **I**) to calculate p values. *p<0.05, **p < 0.01, Scale bars, 100 μm.

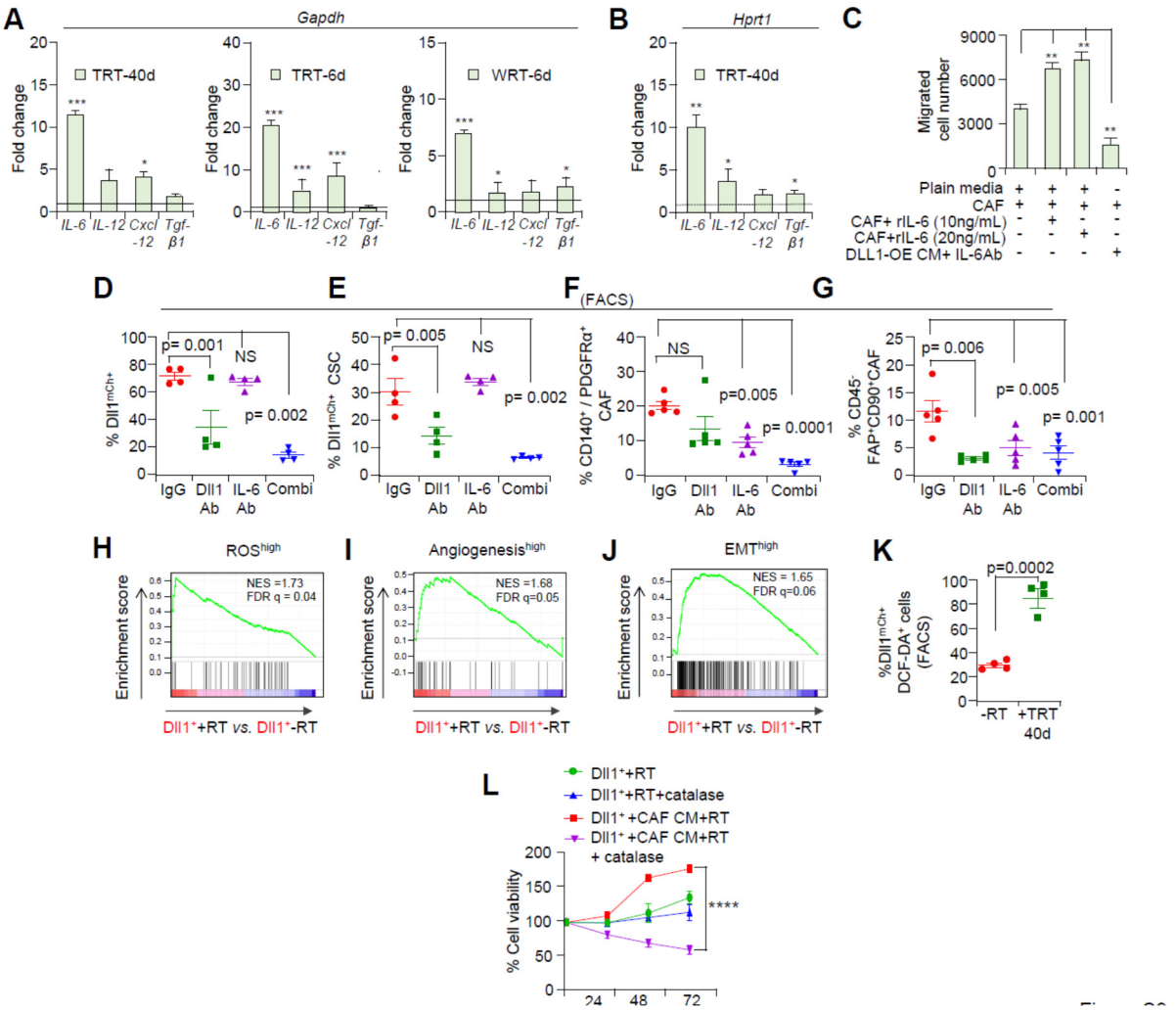

Figure S9. Irradiated Dll1⁺ tumor cells express high IL-6 protein and pharmacological inhibition of IL-6 along with blocking of Dll1 significantly reduces CSC and CAF population. (**A** and **B**) Quantitative PCR (qPCR) analyses with irradiated Dll1⁺ tumor cells show increased expression of *IL-6*, *IL-12* and *Cxcl-12* upon long-term (left panel), short-term targeted radiation (TRT) (middle panel) and short-term whole-body radiation (WRT-6d) (right panel). QPCR values were normalized to *Gapdh* (**A**) and *Hprt1* (**B**). The dashed line represents the relative expression of non-irradiated Dll1⁺ tumor cells and was considered as a fold change of one. Data representative of minimum of two independent experiments with technical duplicates. (**C**) Bar graphs demonstrate total number of migrated CD140⁺/PDGFRα⁺ CAFs sorted from Py-Dll1^{WT} tumors in the presence of indicated conditioned media from tumor cells alone or in

combination with either IL-6 monoclonal antibody (10ng/ml) or IL-6 recombinant (10 ng/ml and 20 ng/ml). (**D-G**) Flowcytometry analyses depict decreased $Dll1^{mCh+}$ tumor cells (**D**) and double positive $Dll1^{mCh+}$ CSC ($Dll1^{mCherry+}CD24^{-}CD44^{+}$) cells in +TRT $Dll1^{+}$ tumors after pharmacological blocking of Dll1 alone or in combination with IL-6 antibody compared to IgG control $Dll1^{+}$ tumors. (n=4 tumors/group). (**F** and **G**), Scatter plots from flowcytometry analyses showing number of $CD140^{+}$/PDGFRα^{+} CAFs (**F**) and $CD45^{-}FAP^{+}CD90^{+}$ CAFs (**G**) in +TRT $Dll1^{+}$ tumors upon indicated *in vivo* treatments (n=5 tumors/group). Each dot in the scatter plot represents individual tumors per group. (**H-J**) GSEA demonstrates enriched ROS signature (**H**), enriched angiogenesis signature (**I**) and enriched epithelial-mesenchymal transition (EMT) signature (**J**) in $Dll1^{+}$ tumor cells after radiation. NES, normalized enrichment score and FDR, false discovery rate. (**K**) Scatter plot represents higher intracellular ROS production as observed by increase in DCF-DA^{+} cells in +TRT $Dll1^{+}$ tumors relative to -RT $Dll1^{+}$ tumors. (**L**) Line graph showing decrease in cell viability of tumor cells after exogenous treatment of catalase (25 units/ml) when tumor cells co-cultured with sorted CAFs condition media (CM). Data are presented as the mean ± SEM. Two-way ANOVA with Bonferroni post-test adjustment (**L**) and unpaired student's *t* test (**A, B** and **K**) and One-way ANOVA with TUKEY test (**C-G**) was used calculate p values. *p<0.05, **p < 0.01, ***p < 0.001, ****p<0.0001, NS=not significant.

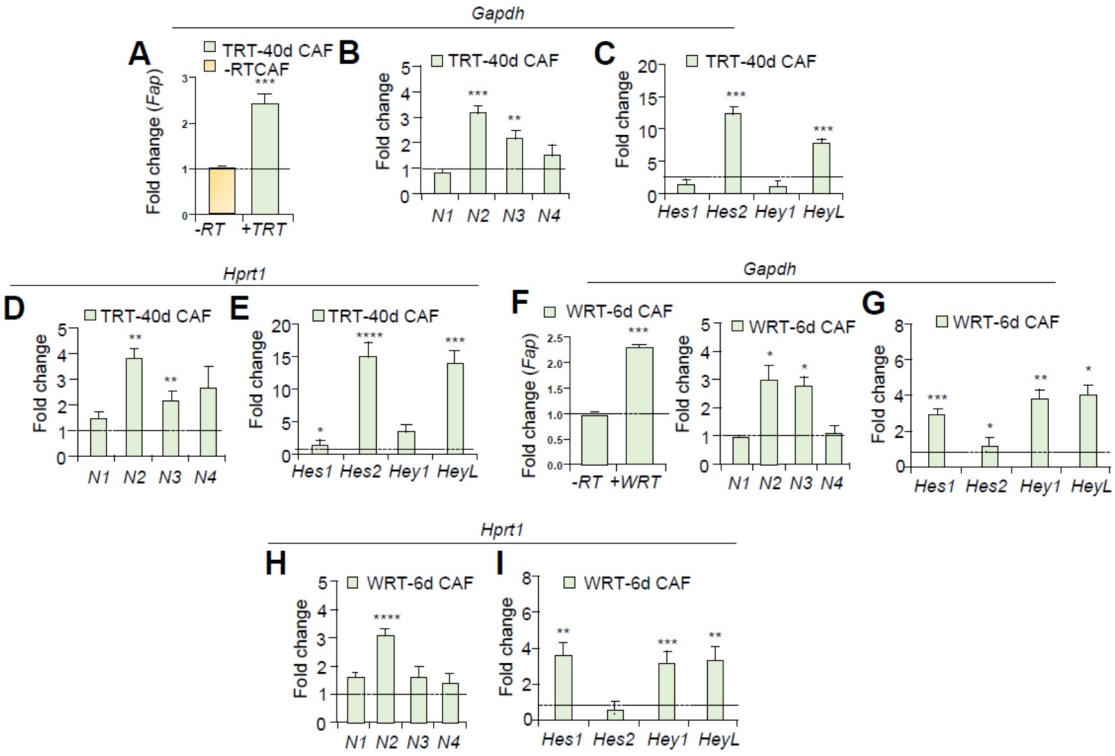

Figure S10. Post irradiated CAFs in tumors express higher Notch receptors and Notch target genes. (**A-E)** Quantitative PCR (qPCR) analyses with sorted CD140^{+}/PDGFRα^{+} CAF population show increased fold change in expression of *Fap* and Notch signaling receptors such as *Notch2* (*N2*) and *Notch3* (*N3*) and downstream Notch target genes such as *Hes1, Hes2, Hey1* and *HeyL* compared to -RT CAFs. The dashed line represents the relative expression of sorted CD140^{+}/PDGFRα^{+} CAF population from -RT Dll1^{+} tumors and was considered as a fold change of one. qPCR values were normalized to *Gapdh* (**A-C**) and *Hprt1* (**D** and **E**). (**F-I**) Quantitative PCR (qPCR) analyses with sorted CD140^{+}/PDGFRα^{+} CAF population from WRT show higher expression of *Fap, Notch2 (N2)* and *Notch3 (N3)* and downstream Notch target genes when qPCR values were normalized to *Gapdh* (**F** and **G**) and *Hprt1* (**H** and **I**). The dashed line represents the relative expression of sorted CD140^{+}/PDGFRα^{+} CAF population from -RT Dll1^{mCh+} tumors and was considered as a fold change of one. Data representative of minimum of two independent experiments with technical duplicates **(A-I)**. Data are presented as the mean ± SEM

(A-I). Unpaired student's *t* test was used calculate p values **(A-I)**. *p<0.05, **p < 0.01, ***p < 0.01, ****p<0.0001.

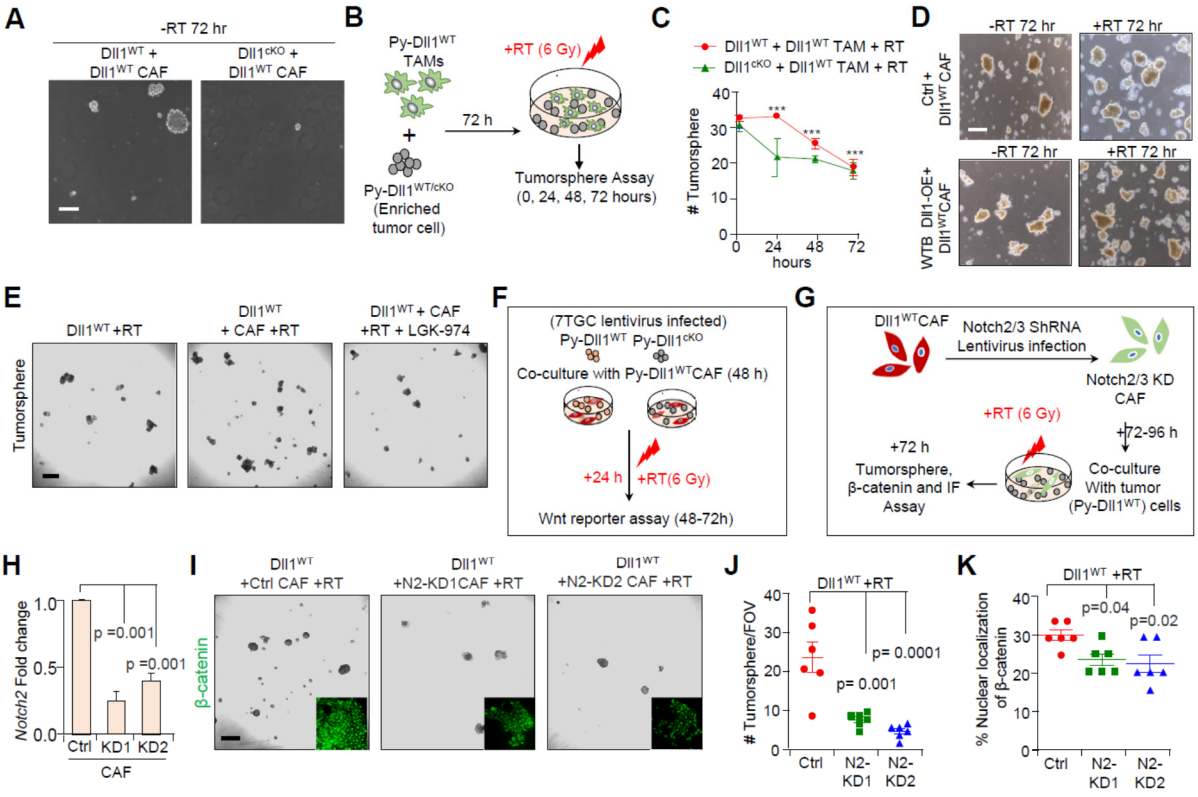

Figure S11. Cancer associated fibroblasts (CAFs) but not tumor associated macrophages (TAMs) promote stemness of Dll1^{+} tumor cells via activation of Wnt signaling after radiation. (**A**) Representative phase contrast images show tumorsphere formed by sorted Py-Dll1^{WT} or Py-Dll1^{cKO} tumor cells when co-cultured with sorted CAFs from Py-Dll1^{WT} tumors. (**B**) Schematic representation depicts the experimental plan of co-culture of tumor associated macrophages (TAMs) and tumor cells (either derived from Py-Dll1^{WT} or Py-Dll1^{cKO} tumors) in 1:2 ratio (total number of 5,000 TAMs and 10,000 tumor cells) tumorsphere condition in low–adherent plate for 72 hours after which the cells were irradiated with single dose of 6 Gy. Spheres were counted in indicated three time points. (**C**) Line graph shows number of tumorsphere formed when Py-Dll1^{WT} and Py-Dll1^{cKO} cells were co-cultured with WT TAMs at different time points post radiation. (**D**) Representative phase contrast images show tumorsphere formed by control WTB cells (with low Dll1 level) and DLL1-overexpressing (OE) (with high Dll1 level) WTB cells when co-cultured with sorted Py-Dll1^{WT} CAFs pre and post radiation. (**E**) Representative phase contrast

images showing post RT, Py-Dll1^{WT} tumor cell-derived tumorsphere count decrease when co-cultured with CAF upon treatment with LGK-974 (10 μM) compared to without LGK-974 treated group. (**F**) Schematic diagram showing method of co-culturing 7TGC infected Py-Dll1^{WT} and Py-Dll1^{cKO} cells with sorted CAF cells (CD140^{+}/PDGFRα^{+}) from Py-Dll1^{WT} tumors. Py-Dll1^{WT} and Py-Dll1^{cKO} tumor cells were stably infected with 7TGC lentivirus to express Wnt reporter as seen by mCherry^{+}/GFP^{+} expression. The expression of mCherry was used to normalize infection efficiency. Equal number of Py-Dll1^{WT} and Py-Dll1^{cKO} tumor cells were co-cultured with CAFs. (**G**) Schematic diagram represents experimental plan of knockdown *Notch2* and *Notch3* genes in CAFs, followed by co-culture with Py-Dll1^{WT} tumor cells post radiation and performed tumorsphere and IF assay. (**H**) Quantitative PCR (qPCR) shows stable knockdown of *Notch2* in CAFs. Two independent shRNAs were used to knockdown *Notch2 (N2)* (KD1 and KD2). qPCR values were normalized to *Gapdh.* (**I-K**) Representative phase contrast images of tumorsphere images (**I**), and β-catenin IF images (inset) and scatter plots (**J** and **K**) showing decrease in number of tumorsphere and nuclear β-catenin expression when Py-Dll1^{WT} cells co-cultured with *Notch2* knocked down CAFs post radiation. All tumorsphere experiments were repeated twice using technical duplicates. Data are presented as the mean ± SEM. Two-way ANOVA with Bonferroni post-test adjustment (**C**) and one-way ANOVA with TUKEY test (**H**, **J** and **K**) were performed to calculate p values. Scale bars, 500 μm (**A**, **D**, **E** and **I**) and 100 μm (**I**; insets). FOV =field of view

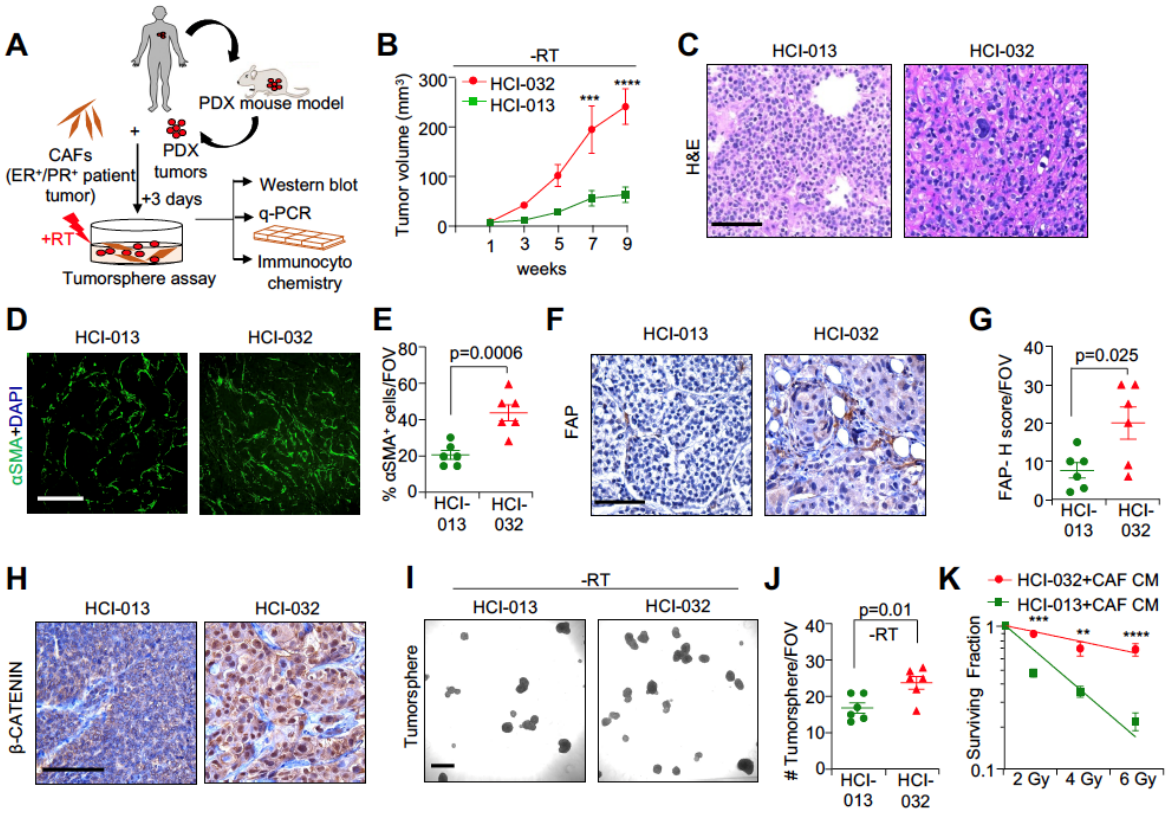

Figure S12. Aggressive luminal human patient derived xenografts (PDX) have higher CAF infiltration and high stem cell function. (**A**) Schematic diagram represents experimental plan for co-culture of total 4,000 CAFs (sorted from ER$^+$/PR$^+$ human breast tumors) and total number of 10,000 PDX tumor cells plated in low–adherent plate for 3 days, after which the cells were irradiated with single dose of 6 Gy followed by counting, western blot, qPCR and immunocytochemistry at 72h. (**B**) Luminal human patient derived xenograft (HCI-013 and HCI-032) tumor chunks were implanted into mammary fat pad of immunocompromised NCG mice (obtained from Charles River Laboratories), and tumor growth was observed by weekly palpation. Representative tumor growth curves show increase tumor progression in HCI-032 compared to HCI-013 tumors. (**C**) Representative hematoxylin and eosin (H&E) images show high abundance of large nuclei tumor cells and stroma in aggressive HCI-032 tumors compared to less aggressive HCI-013 PDX. (**D-G**) Representative IF images and quantification indicate higher αSMA$^+$ myCAFs (**D** and **E**) and representative IHC images and quantification (**F** and **G**) indicate FAP$^+$ expressing

CAFs in aggressive HCI-032 PDX tumors compared to less aggressive HCI-013 PDX tumors. **(H)** Representative IHC images show more nuclear β-catenin expression in HCI-032 PDX tumors compared to HCI-013 PDX tumors. (**I** and **J**) Representative phase contrast images and scatter plot depict HCI-032 PDX forms significant higher number of tumorspheres relative to HCI-013 PDX. (**K**) Clonogenic survival assay graph showing greater percentage of surviving fraction of HCI-032 PDX tumor cells than HCI-013 PDX tumor cells when cultured with condition media (CM) from sorted $CD140^{+}$/$PDGFR\alpha^{+}$ human CAF after radiation. Data are presented as the mean ± SEM. Two-way ANOVA with Bonferroni post-test adjustment was performed to calculate p values (**B**). Unpaired student's *t* test was used calculate p values (**E**, **G**, **J** and **K**). **p<0.01, ***p < 0.001, ****p<0.0001. Scale bars, 100 μm (**C**, **D**, **F** and **H**), 500μm (**I**). FOV =field of view

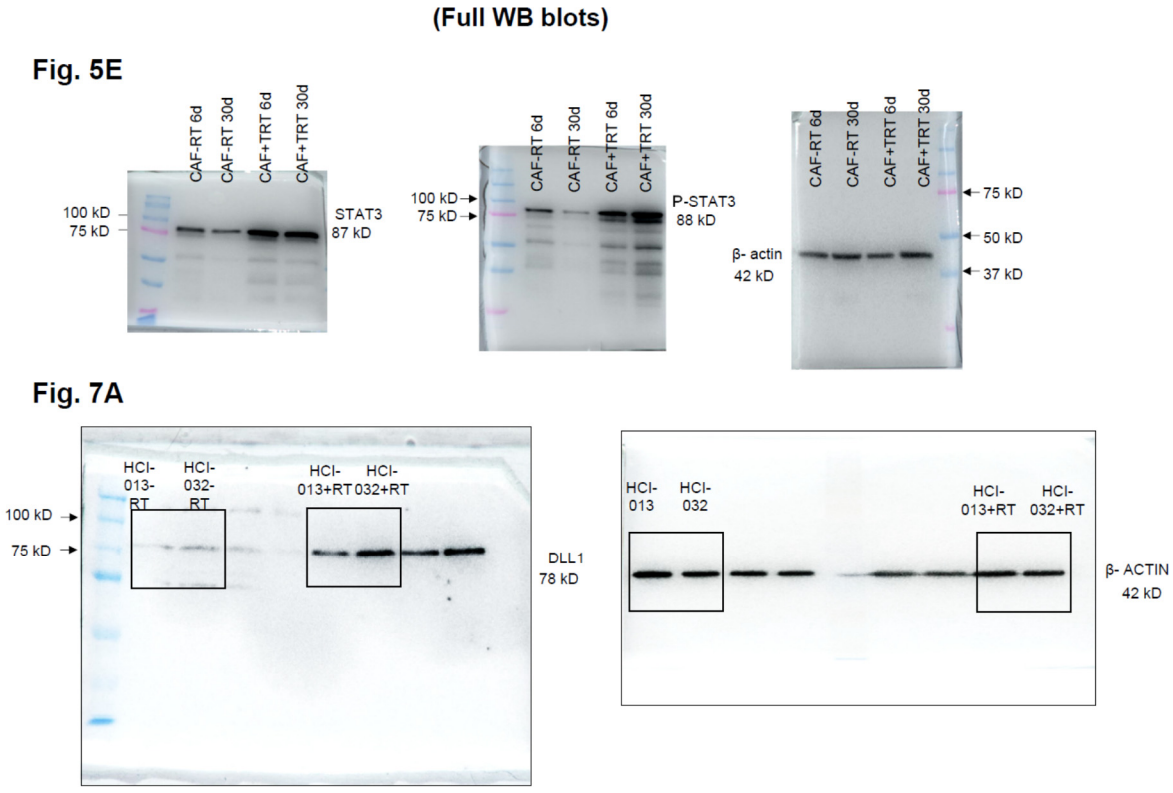

Figure S13. Uncropped western blots

Additional methods:

Human studies

The intensity of immunohistochemistry (IHC) staining was measured using the scale 0–3, 0 being negative and 3 being very high expression. The abundance of positive cells in the tissue was measured using a scale ranging from 0 to 100. An intensity score of more than 1 was considered as positive cells to score abundance. For immunofluorescence (IF) staining, the abundance of the positive cells was calculated in percentage per field of view (FOV). Human slides were evaluated by board-certified clinical breast cancer pathologist. For patient derived xenograft (PDX) studies, $ER^+/PR^+/HER2^-$ HCI-013 and HCI-032 PDXs were used. All information for PDX samples is available in published report from A. Welm's Laboratory (1).

Metastatic nodules count and quantification by flow cytometry

For Py-Dll1^{mCh+} mice, after a brief wash with Phosphate- Buffered Saline (PBS), the Dll1^{mCh+} nodules in lungs were imaged and counted under a Leica fluorescent dissection microscope. After imaging, the lungs were processed following the published procedure(2) to count metastatic nodules. Lungs were then fixed with Bouin's solution for 24 hours, washed twice with 70% ethanol and then counted for metastatic nodules based on whole lung images. For Py-Dll1^{mCh-}, Py-Dll1^{WT} and Py-Dll1^{cKO} mice, the lungs were directly fixed with Bouin's solution for 24 hours and then washed twice with 70% ethanol and then counted for nodules based on whole lung images using the dissection microscope.

For flow cytometric quantification of Dll1^{mCh+} tumors cells in blood, 500 µL of blood was isolated from Py-Dll1^{mCh} tumor-bearing mice of different groups at end point. Red blood cells (RBCs) were removed using 0.64% sterile ammonium chloride solution for 5 min at 37 °C. Cells were then analyzed based on mCherry (Dll1) expression. To quantify Dll1^{mCh+} tumor cells in the bone marrow, bone marrow was flushed and collected using mammary epithelial cell Growth Medium (MEGM), supplemented with growth factors (3) and subsequently assessed by flowcytometry for mCherry (Dll1) expression. Sterile bone marrow cells were further cultured in tissue culture dishes for 5-7 days in MEGM and Dll1^{mCh+} tumor cells were imaged using a Nikon TiE microscope.

Flow Cytometric Analysis (FACS) and Sorting

Single cells from tumor (4) were stained with a combination of antibodies (listed in the Supplemental Table S3) following established protocol. Tumor cells were enriched after removal of RBC, CD31^{+} endothelial and CD45^{+} leukocytes cells. For isolation of murine cancer associated fibroblast (CAF), CD140/PDGFRα and F4/80 antibodies were used to get F4/80^{-} CD140^{+}/PDGFRα^{+} (henceforth, referred to as CD140^{+}/PDGFRα^{+} CAFs) while for human CAF isolation, we used EPCAM and CD140/PDGFRα antibodies to get CD140^{+}/PDGFRα^{+} CAFs

(henceforth, referred to as CD140^{+}/PDGFRα^{+} CAFs). An LSRII/Fortessa and Aria II Flow Cytometers (BD Biosciences) were used for all flow-based experiments. Flow Jo software (Tree Star, Inc) was used for analysis. Antibodies used are listed in the Supplemental Table S3.

Clonogenic survival assay

Briefly, primary tumor cells from either Py-Dll1$^{mCh+/-}$, Py-Dll1$^{WT/cKO}$ or PDX tumor cells (HCI-013 and HCI-032) were cultured with CM of CAFs. After seeding, cells were incubated overnight to facilitate adherence. On the following day, the plates were irradiated at 0, 2, 4 and 6 Gy for each different groups. The percentage of surviving fraction was calculated using the following formula- [(colonies formed in three (triplets) petri dishes for each dose level irradiated/ number of cells seeded) x100] (5).

MTT assay

Sorted Dll1^{mCh+} cells were seeded at a density of 1x10^{4} cells/well and cultured with condition media (CM) from sorted CAF in 200 µL DMEM supplemented with 10% FBS and catalase (25 units/ml) (Millipore, catalog no. C9322-1G) respectively in 96-well plates 24, 48 and 72 hours following radiation. For MTT assay, cells were treated with MTT reagent as previously described (6).The assay was performed in triplicate and the relative cell viability (%) was expressed as a percentage relative to the untreated control cells.

Viral infection and Wnt reporter assay

For lentivirus-mediated knockdown studies, shRNA constructs for *Notch2* (TRCN0000340512, TRCN0000340513) and for *Notch3* (TRCN0000075572, TRCN0000075569) were obtained from Sigma-Aldrich. Empty pLKO.1 vector from Sigma-Aldrich was used as control as a backbone vector for all Notch3 shRNAs. Empty pLKO.2 vector from Sigma-Aldrich was used as control as a backbone vector for Notch2 shRNAs. We used previously described Dll1 overexpression

construct (2), in which Dll1 cDNA was cloned into pLEX MCS plasmid (Open Biosystems) (7). Stable 7TGC-Py-Dll1^{WT} and 7TGC-Py-Dll1^{cKO} primary tumor cell lines and 7TGC-HCI-013 and 7TGC-HCI-032 PDX cell lines were made using 7TGC plasmid (Addgene, catalog no. 24304) (8). All plasmids were packaged into virus using HEK293-T cells as standard protocols (9). WTB cell line, stable primary tumor cell lines and CAFs were plated and infected with virus-containing media supplemented with 2 µg/ml polybrene (Sigma-Alrich, catalog no. H9268) for minimum of 48 hours. After infection, media were replaced with fresh media containing puromycin (Millipore, Sigma, catalog no. MABE343) for selection of the virus-infected cells.

For Wnt reporter assay, stable 7TGC-Py-Dll1^{WT} and 7TGC-Py-Dll1^{cKO} primary tumor cell lines and 7TGC-HCI-013 and 7TGC-HCI-032 PDX cells were plated at 5x10^5 cells per well in the six-well plates. Cells were trypsinized approximately 72 hours post irradiation and Wnt reporter activity (GFP expression) were measured by flowcytometry. Relative Wnt reporter activity was determined by normalizing GFP to mCherry expression.

Migration assay

Transwell inserts (8-µm pore size; Corning Incorporated, Corning, NY, USA) were used for Boyden-chamber assay to assess CAFs migration after 7 hours. A total of 35,000 sorted CAF cells were added in 500 µL of serum free medium into the upper chamber whereas the lower chamber was filled with Dulbecco's modified Eagle's medium (DMEM), containing IL-6 recombinant protein (rIL-6). Two doses (10 ng/ml and 20 ng/ml) of rIL-6 were used (Shenandoah Biotechnology, catalog no. 200-02-10UG). In addition, anti-IL-6 monoclonal antibody (10 ng/ml) (Bioxcell, catalog no. BE0046) was used in the conditioned media (indicated legends).

Histological, Immunohistochemistry (IHC) and immunofluorescence (IF) analyses

For histological analyses, mouse tumor specimens were processed as previously described (9). Antibodies information and dilutions are listed in the Supplemental Table S3. For IF analysis from co-culture experiment setting, cells in suspension were attached to chamber slides. 24-48 hours post culture in serum containing media, cells were fixed with 4% paraformaldehyde on ice for 15 mi. Cells were then permeabilized with 0.01% 1X Triton-X solution for 15 min at room temperature. Images were taken using a Nikon TiE Microscope and Leica SP5 FLIM Confocal microscope and several fields of view (FOV) were taken for each sample. Multiple samples were used for scoring per group/experiment. Antibodies used are listed in the Supplemental Table S3.

ELISA

Tumor tissues isolated either 6 or ~40 days after TRT were enzymatically digested as described previously. The levels of IL-6 production in sorted F4/80^{-} CD140^{+} (PDGFR-α^{+}) CAFs were assayed using ELISA kits according to the instructions provided by the manufacturer (Thermo-fisher Scientific, catalog no. KMC0061) in an ELISA plate reader (Biotek, USA).

Measurement of intracellular Reactive Oxygen Species (ROS) production

The amount of DCF is proportional to the amount of ROS present inside the cell. Briefly, Dll1^{mCh+} tumor cells were sorted from control and irradiated tumors post 6 day and ~40 days of targeted radiation by flowcytometry and were incubated with 20 μM DCFH-DA working solution for 60 min in the dark at 37 °C. Finally, cells were suspended in flowcytometry buffer, and ROS generation was measured using a Fortessa Flow Cytometer (BD Biosciences) in accordance with the manufacturer's instructions.

Protein extraction and western blot analysis

For Western blot analysis, whole cell extracts from mouse tumors and cell extracts from co-culture experiments (Patient derived xenografts (PDX) tumor cells with or without RT) was prepared as

previously described (2) . HRP tagged anti-β-actin antibody was used as a loading control for 1 hour at room temperature. Antibodies used are listed in the Supplemental Table S3. Uncropped western blot images are shown in the Supplementary Fig. S13.

RNA extraction and quantitative PCR (qPCR)

Total RNA was isolated from sorted tumor cells or CAFs using the Invitrogen RNA extraction kit (Thermo Scientific, catalog no. 12183018A) in accordance with the manufacturer's instructions. Quantitative real-time (qPCR) was performed on the Applied Biosystems Quantstudio PCR machine (Thermo Fisher) using SYBR Green Power (Life Science Technologies). The gene-specific primer sets were used at a final concentration of 0.2 μM and their sequences are provided in Supplementary Table S4.

ScRNA-seq

Sorted $CD45^-$ $Dll1^+$ and $Dll1^-$ tumor cell suspensions were loaded on the 10x Genomics Chromium Controller Single-Cell Instrument (10x Genomics) and sequencing libraries were constructed using the reagents provide in the Chromium Single-Cell 3′ Library Kit following the user guide. Sequencing libraries were sequenced with the Illumina platform. The scRNA-sequenced $CD45^-$ $Dll1^+$ and $Dll1^-$ datasets were then merged and analyzed using Seurat. Counts were log-normalized and scaled, and the top 20 principal components were used for graph-based clustering and visualization with uMAP.

Bulk mRNA-Sequencing

Bulk mRNA sequencing was performed by Novogene. All steps for library construction were carried out according to the NEBNext® Ultra™ II Non-Directional RNA Library Prep Kit for Illumina® (New England BioLabs Inc., Massachusetts, USA) as described in manufacture's protocol. Equimolar pooling of libraries was performed based on QC values and sequenced on

an Illumina® NovaSeq (Illumina, California, USA) with a read length configuration of 150 PE for 40 M PE reads per sample (20M in each direction).

1. DeRose YS, Wang G, Lin YC, Bernard PS, Buys SS, Ebbert MT*, et al.* Tumor grafts derived from women with breast cancer authentically reflect tumor pathology, growth, metastasis and disease outcomes. Nat Med **2011**;17:1514-20
2. Kumar S, Srivastav RK, Wilkes DW, Ross T, Kim S, Kowalski J*, et al.* Estrogen-dependent DLL1-mediated Notch signaling promotes luminal breast cancer. Oncogene **2019**;38:2092-107
3. Chakrabarti R, Wei Y, Hwang J, Hang X, Andres Blanco M, Choudhury A*, et al.* DeltaNp63 promotes stem cell activity in mammary gland development and basal-like breast cancer by enhancing Fzd7 expression and Wnt signalling. Nat Cell Biol **2014**;16:1004-15, 1-13
4. Kumar S, Wilkes DW, Samuel N, Blanco MA, Nayak A, Alicea-Torres K*, et al.* DeltaNp63-driven recruitment of myeloid-derived suppressor cells promotes metastasis in triple-negative breast cancer. J Clin Invest **2018**;128:5095-109
5. Wang H, Zhang X. ROS Reduction Does Not Decrease the Anticancer Efficacy of X-Ray in Two Breast Cancer Cell Lines. Oxid Med Cell Longev **2019**;2019:3782074
6. Kumar S, Nandi A, Singh S, Regulapati R, Li N, Tobias JW*, et al.* Dll1(+) quiescent tumor stem cells drive chemoresistance in breast cancer through NF-kappaB survival pathway. Nat Commun **2021**;12:432
7. Chakrabarti R, Celia-Terrassa T, Kumar S, Hang X, Wei Y, Choudhury A*, et al.* Notch ligand Dll1 mediates cross-talk between mammary stem cells and the macrophageal niche. Science **2018**;360
8. Fuerer C, Nusse R. Lentiviral vectors to probe and manipulate the Wnt signaling pathway. PLoS One **2010**;5:e9370
9. Chakrabarti R, Hwang J, Andres Blanco M, Wei Y, Lukacisin M, Romano RA*, et al.* Elf5 inhibits the epithelial-mesenchymal transition in mammary gland development and breast cancer metastasis by transcriptionally repressing Snail2. Nat Cell Biol **2012**;14:1212-22

Table S1. Details of human patient samples

(ER^+/PR^+) luminal patient sample details (No radiation treatment -RT)									
Patient ID	**A/R/S**	**Diagnosis Date**	**Date of death (IA)**	**Radiation TX(Y/N)**	**Recurrence (Y/N)**	**Site and date of recurrence**	**Months after RDX**	**Chemo (Y/N)**	**Type of chemo**
90361	35/W/F	May-07	unknown	N	Y	Lymph node-7/2009	N/A	Y	Adriamycin and cyclophosphamide and Taxol
90362	64/W/F	Oct-07	unknown	N	Y	Lymph node-11/2007	N/A	Y	Unknown chemo type
90363	42/W/F	Jan-08	unknown	N	N	N/A	N/A	N	No
90364	62/W/F	Aug-08	unknown	N	N	N/A	N/A	Y	Adriamycin and cyclophosphamide and Taxol
90365	95/W/F	Jan-08	Mar-08	N	N	N/A	N/A	N	No
90366	44/W/F	Jul-08	unknown	N	N	N/A	N/A	Y	Taxotere, Cytoxan, tamoxifen
90367	79/W/F	Jul-08	Apr-19	N	N	N/A	N/A	Y	Femara, anastrozole
90368	52/W/F	Apr-09	unknown	N	N	N/A	N/A	Y	Adriamycin and cyclophosphamide, taxol and avastin
90267	60/W/F	Aug-20	unknown	N	N	N/A	N/A	N	No
90369	50/W/F	Jun-09	unknown	N	Y	Breast 6/2018	N/A	Y	Zoladex, anastrozole

90370	40/W/F	Jul-09	unknown	N	Y	Breast 6/2018	N/A	Y	Unknown
88419/88420	82/W/F	Nov-15	Unknown	N	N	N/A	N/A	N/A	N/A
88423/88424	69/W/F	Jul-05	unknown	N	N	N/A	N/A	N/A	N/A
88430/88431	93/W/F	Sep-15	Aug-17	N	N	N/A	N/A	N/A	N/A
88434/88345	79/W/F	Apr-16	unknown	N	N	N/A	N/A	N/A	N/A
88444/88445	90/W/F	Dec-16	unknown	N	N	N/A	N/A	N/A	N/A
88448/88449	49/A/F	Dec-16	unknown	N	N	N/A	N/A	N/A	N/A
(ER^+/PR^+) luminal patient sample details (Neoadjuvant setting +NART)									
90551	78/W/F	Jun-17	Jun-17	Y	Y	Lymph node-6/2017	3	N	No
90552	35/W/F	Aug-17	unknown	Y	Y	Lymph node-8/2017	6	Y	Toxotere and Cytoxan
90554	66/W/F	Oct-17	unknown	Y	N	N/A	7	Y	Adriamycin, cyclophosphamide and taxol
90555	50/B/F	Feb-18	unknown	Y	Y	Lymph node-2/2018	7	Y	Toxotere and Cytoxan

88482	48/AS/F	Apr-19	unknown	Y	N	N/A	4	Y	Taxotere, carboplatin, Herceptin, Perjeta, Trastuzumab, tamoxifen
83526	66/B/F	Nov-12	unknown	Y	Y	Breast-2017	5	Y	Trastuzumab, Carboplatin, docetaxel
90124	67/W/F	Aug-20	unknown	Y	N	N/A	10	Y	Toxotere and Cytoxan
88440/88441	72/W/F	Jun-05	unknown	Y	Y	Breast 7/2016	4	N	No
88442/88443	53/W/F	Dec-16	unknown	Y	N	N/A	3	Y	Taxotere, carboplatin, Herceptin, Perjeta, Trastuzumab, tamoxifen
90356	60/W/F	Jan-10	Mar-12	Y	Y	Lymph node 5/2011	6	Y	Adriamycin and cyclophosphamide and Taxol
83012	75/W/F	Jul-17	unknown	Y	N	N/A	4	Y	Taxol
88989	41/B/F	Mar-19	Mar-20	Y	Y	Lung	3	Y	Cyclophosphamide and Taxol
(ER^+/PR^+) luminal patient sample details (adjuvant setting +ART)									

90553	78/W/F	Jul-15	unknown	Y	Y	Spine/lung 7/2015	11	Y	Femara, Fulvestrant/Palbociclib
82543	50/HIS/F	Mar-17	Dec-18	Y	Y	T5 Vert 3/2018	6	Y	Cyclophosphamide, taxol, Herceptin and Doxo-rubicin
82743	64/W/F	Jun-17	unknown	Y	Y	N/A	6	Y	Toxotere, Carboplatin, Herceptin. Perjeta
83252	71/W/F	Nov-17	Jan-21	Y	Y	Brain 9/20, Temporal bone 8/2018 , bone mets 7/2019	5	N	No

(ER^-/PR^-) TNBC patient sample details (without radiation -RT)

Patient ID	A/R/S	Diagnosis Date	Date of death (IA)	Radiation TX(Y/N)	Recurrence (Y/N)	Site and date of recurrence	Months after RDX	Chemo (Y/N)	Type of chemo
90351	90/W/F	Aug-07	Dec-07	N	Y	Spine 11/2007	N/A	Y	Unknown
90352	50/W/F	Jul-05	Unknown	N	N	N/A	N/A	Y	Femara
90353	51/W/F	June-09	Unknown	N	N	N/A	N/A	Y	Docetaxel, Carboplatin, Trastuzumab
90354	46/H/F	Aug-09	Apr-10	N	Y	Breast 3/2010	N/A	Y	unknown

90357	76/W/F	Nov-13	Nov-15	N	N	N/A	N/A	Y	Taxotere/ Cytoxan
90358	82/H/F	Apr-15	May-19	N	N	N/A	N/A	Y	Unknown
90405	69/B/F	Sep-20	Unknown	N	Y	Liver/lung-9/2020	N/A	N	N/A
90371	93/W/F	Aug-20	Unknown	N	N	N/A	N/A	N	N/A
90355	72/W/F	Dec-09	Unknown	N	N	N/A	N/A	Y	Adriamycin and cyclophosphamide

90356	60/W/F	Jan-02	Mar-12	N	Y	Lymph node 5/2011	N/A	Y	Adriamycin and cyclophosphamide, taxol
90359	86/W/F	Apr-16	Unknown	N	N	N/A	6	Y	Cyclophosphamide, methotrexate Floorouracil
90360	81/W/F	Nov-15	Jun-17	Y	N	N/A	12	Y	Cyclophosphamide, Methotrexate Fluorouracil
(ER^-/PR^-) TNBC patient sample details (neoadjuvant setting +NART)									
62917	64/W/F	Aug-21	Oct-21	Y	Y	Lung 9/2015	3	Y	Cyclophosphmide

90556	66/W/F	Oct-17	Unknown	Y	N	N/A	7	Y	Adriamycin and cyclophosphamide, taxol
90557	50/B/F	Feb-18	Unknown	Y	Y	Lymph node 2/2018	7	Y	Taxotere and Cytoxan
90548	66/W/F	Jun-17	Unknown	Y	N	N/A	9	Y	Adriamycin and cyclophosphamide
90549	69/W/F	Jun-17	Unknown	Y	N	N/A	9	Y	Adriamycin and cyclophosphamide
(ER^-/PR^-) TNBC patient sample details (adjuvant setting +ART)									

81210	59/W/F	Jan-12	Unknown	Y	N	N/A	3	Y	Unknown
90546	78/W/F	Oct-16	Unknown	Y	N	N/A	5	Y	Adriamycin and cyclophosphamide, taxol
90547	52/W/F	Nov-16	Unknown	Y	N	N/A	6	Y	Adriamycin and cyclophosphamide, taxol

Table S2A. Several enriched signaling pathways associated with radiation signature in Dll1$^+$ tumor cells after radiation.

Pathway name **Dll1$^+$ +RT vs Dll1$^+$ -RT**	**NOM** **P value**	**FDR-q** **value**
Rashi_response_to_ionizing_radiation_6	0.000	0.002
KYNG_DNA_damage_by_gamma_radiation	0.015	0.101
Ghandhi_bystander_irradiation_up	0.025	0.148
TSAI_response_to_ionizing_radiation	0.052	0.235

Table S2B. Bulk mRNA seq analysis showing most differentially expressed and upregulated genes in CAFs from tumors after 6 days of targeted radiation (TRT) (left panel) and whole-body radiation (WRT) (right panel)

Gene name **Ctrl CAF vs** **TRT 6d CAF**	**Fold** **Change**
Wnt5b	5.276887
Wnt7b	4.2778
Wnt4	5.502852
Wnt2	3.219189
Wnt7a	1.154315
Wnt8b	1.197427

Gene name **Ctrl CAF vs** **WRT 6d CAF**	**Fold** **Change**
Wnt4	8.036606
Wnt7b	1.985043
Wnt5a	1.423538
Wnt11	1.786107

Table S3. Details of antibodies used for flowcytometry (FACS), Immunohistochemistry (IHC), Immunofluorescence (IF) and Western blot (WB)

Reagent or Resource	Source	Identifier
PE Rat Anti-mouse CD24 FACS (1: 100 for analysis and 1:50 for sorting)	BD Biosciences	Cat# 553262, RRID: AB_394741
APC Rat anti mouse CD44 FACS (1:100 for analysis)	BD Biosciences	Cat# 559250, RRID: AB_398661
FITC Hamster Anti-Mouse CD29 FACS (1:50 for sorting)	Bio-Rad	Cat# MCA2298F, RRID: AB_566688
Biotin Rat Anti-CD31 FACS (1:50 for sorting)	BD Biosciences	Cat# 558737, RRID: AB_397096
Biotin Rat Anti-Mouse CD45 FACS (1:50 for sorting)	BD Biosciences	Cat# 553078, RRID: AB_394608
Biotin Rat Anti-Mouse TER-119 FACS (1:50 for sorting)	BD Biosciences	Cat# 553672, RRID: AB_394985
PE-Cy7 Streptavidin FACS (1:50 for sorting)	Thermo Fisher Scientific	Cat# 25-4317-82, RRID: AB_10116480
APC Rat Anti-mouse CD140 (PDGFRα) FACS (1:100 for analyses and 1:50 for sorting)	Thermo Fisher Scientific	Cat# 17-1401-81, RRID: AB_529482

PE-Cyanine7 Rat Anti-mouse CD140 (PDGFRα)-APA5 FACS (1:100 for analysis)	Thermo Fisher Scientific	Cat# 25-1401-82, RRID: AB_2573400
PE/Cyanine7 anti-human CD140 (PDGFRα)-APA5 FACS (1: 50 for sorting)	Biolegend	Cat# 323507, RRID: AB_2565596
FITC anti-human CD326 (EPCAM) Antibody FACS (1:50 for sorting)	Biolegend	Cat# 324203, RRID: AB_ 756077
APC/Cy7 anti-mouse F4/80 FACS (1:50 for sorting)	BD Biosciences	Cat# 123118, RRID: AB_893477
PE Rat Anti-mouse CD90 FACS (1:100 for analysis)	Invitrogen	Cat# 12-0900-81, RRID: AB_465773
PE-Cy7 Rat Anti- mouse CD45 FACS (1:100 for analysis)	BD Biosciences	Cat# 552848, RRID: AB_394489
FITC Anti-alpha Smooth muscle actin (αSMA) FACS (1:100 for analysis)	Thermo Fisher Scientific	Cat# 53-9760-80, RRID: AB_2574460
FITC Anti-mouse IL-6 FACS (1:100 for analysis)	Thermo Fisher Scientific	Cat# 11-7061-41, RRID: AB_1633408
Anti-rabbit cytokeratin 14 IHC/IF (1:75)	Abcam	Cat# ab53115, RRID: AB_869856
Anti-rabbit FAP	Abcam	Cat# ab207178, RRID: AB_ 2864720

IHC (1:250), IF (1;50)		
Anti-mouse alpha smooth muscle actin (αSMA) IF (1:150)	Abcam	Cat# ab7817, RRID: AB_ 262054
Anti-rabbit carbonic anhydrase IX (CAIX) IF (1:25)	Abcam	Cat# ab15086, RRID: AB_ 2066533
Anti- rabbit mCherry IF (1:75)	Abcam	Cat# ab167453, RRID: AB_2571870
Anti-rabbit mCherry IF (1:75)	Abcam	Cat# ab183628, RRID: AB_ 2650480
Anti-mouse mCherry IF (1:75)	Abcam	Cat# ab125096, RRID: AB_11133266
Anti-mouse Beta catenin IHC (1:50), IF (1:10)	Thermo Fisher Scientific	Cat#, MA1-301, RRID: AB_1070649
Anti-rabbit DLL1 IHC (1:100)	Abcam	Cat# ab84620, RRID: AB_1860333
Anti-rabbit DLL1 IHC (1:100), WB (1:1000)	Thermo Fisher Scientific	Cat# PA542902, RRID: AB_ 2610508
Anti-rabbit CD163 (EPR19518) IHC (1:100)	Abcam	Cat# ab182422; RRID: AB_ 2753196
Anti-mouse Beta actin, peroxidase WB (1:20000)	Sigma Aldrich	Cat# A3854, RRID: AB_262011
Anti-rabbit Stat-3 (D3Z2G) WB (1:1000)	Cell signaling Technologies	Cat# 12640S, RRID: AB_ 2629499
Anti-rabbit phospho Stat-3 (Tyr705) (D347) WB (1:1000)	Cell signaling Technologies	Cat# 9145T, RRID: AB_ 2491009

Anti-rabbit IgG HRP-linked WB (1:2000)	Cell signaling Technologies	Cat# 7074S, RRID: AB_2099233
Goat anti-rabbit IgG (H+L) Alexa Fluor 594 IF (1:500)	Thermo Fisher Scientific	Cat# A-11012, RRID: AB_2534079
Goat anti-rabbit IgG (H+L) Alexa Fluor 488 IF (1:250)	Thermo Fisher Scientific	Cat# A-21206, RRID: AB_2535792
Goat anti-mouse IgG (H+L), Alexa Fluor 488 IF (1:250)	Thermo Fisher Scientific	Cat# A-11029, RRID: AB_2534088
Goat anti-mouse IgG (H+L), Alexa Fluor 568 IF (1:500)	Thermo Fisher Scientific	Cat# A-11031, RRID: AB_144696

Table S4. Details of primers used for quantitative PCR (qPCR)

Reagent or Resource	Source	Identifier
Fap, Forward 5' CAC CTG ATC GGC AAT TTG TG 3'	This paper	NA
Fap, Reverse 5' CCC ATT CTG AAG GTC GTA GAT GT 3'	This paper	NA
Dll1, Forward 5' GCGAGCTGCACGGACCTTGA 3'	This paper	NA
Dll1, Reverse 5'GCCCAAGGGGCAATGGCAG 3'	This paper	NA
Hes1, Forward 5'CCCCAGCCAGTGTCAACA 3'	This paper	NA
Hes1, Reverse 5'TGTGCTCAGAGGCCGTCTT 3'	This paper	NA
Hes2, Forward 5'GCTACCGGACCAAGGAAGTTC 3'	This paper	NA
Hes2, Reverse5'GAGCTAGACTGTTCTCAAAGTGAGTGA3'	This paper	NA
Hey1, Forward 5'GGGAGGGTCAGCAAAGCA 3'	This paper	NA
Hey1, Reverse 5'GCTGCGCATCTGATTTGTCA 3'	This paper	NA
Hey L, Forward 5'AGATGCAAGCCCGGAAGAA 3'	This paper	NA

Hey L, Reverse 5’CGCAATTCAGAAAGGCTACTGTT 3’	This paper	NA
Notch1, Forward 5’CCAGCAGATGATCTTCCCGTA 3’	This paper	NA
Notch1, Reverse 5’TAGACAATGGAGCCACGGATGT 3’	This paper	NA
Notch2, Forward 5’TCTATCCCCCGTCGATTCG 3’	This paper	NA
Notch2, Reverse 5’GATGTGATCATGGGAGAGGATGT 3’	This paper	NA
Notch3, Forward 5’CCAGGGAATTTCAGGTGCAT 3’	This paper	NA
Notch3, Reverse 5’GCCGTCGAGGCAAGAACA 3’	This paper	NA
Notch4, Forward 5’GAGHACCTGGTTGAAGAATTGATC 3’	This paper	NA
Notch4, Reverse 5’TGCAGTTTTTCCCCTTTTATCC 3’	This paper	NA
IL-6, Forward 5’GCCTTCTTGGGACTGATGCT 3’	This paper	NA
IL-6, Reverse 5’GCCATTGCACAACTCTTTTCTCA 3’	This paper	NA
IL-12, Forward 5’TGGATCTGAGCTGGACCCTT 3’	This paper	NA
IL-12, Reverse 5’GGCCAAAAAGAGGAGGTAGCG 3’	This paper	NA
Cxcl-12, forward 5’GCACTTTCACTCTCGGTCCA 3’	This paper	NA
Cxcl-12, reverse 5’GGTTTACCGTCACTGATGCA 3’	This paper	NA
Tgf-β1, forward 5’GAGGTCACCCGCGTGCTA 3’	This paper	NA
Tgf-β1, reverse 5’TGTGTGAGATGTCTTTGGTTTTCTC 3’	This paper	NA
Axin2, Forward 5’ CCAACGACAGCGAGTTATCC3’	This paper	NA
Axin2, Reverse 5’ TTCTTACTCCCCATGCGGTAA3’	This paper	NA
Ccnd1, Forward 5’ CTCTCCTGCTACCGCACAA 3’	This paper	NA
Ccnd1, Reverse 5’ CTTGACTCCAGAAGGGCTTCA 3’	This paper	NA
Lgr5, Forward 5’ CTCCAACCTCAGCGTCTTCA 3’	This paper	NA
Lgr5, Reverse 5’ ATGTAGGAGACTGGCGGGTA 3’	This paper	NA
Ascl2, Forward 5’ GTAGGTCCACCAGGAGTCAC 3’	This paper	NA
Ascl2, Reverse 5’ CAGGAGCTGCTTGACTTTTCC 3’	This paper	NA
Gapdh, Forward 5’ CCCCAATGTGTCCGTCGTG 3’	This paper	NA
Gapdh, Reverse 5’GCCTGCTTCACCACCTTCT 3’	This paper	NA
Hprt1, Forward 5’CCAACTTTGCTTTCCCTGGT3’	This paper	NA
Hprt1, Reverse 5’TCTGGCCTGTATCCAACACTTC 3’	This paper	NA
AXIN2, Forward 5’ AAGGGCCAGGTCACCAAAC 3’	This paper	NA
AXIN2, Reverse 5’ CCCCCAACCCATCTTCGT 3’	This paper	NA

CCND1, Forward 5’ GCTGCGAAGTGGAAACCATC 3’	This paper	NA
CCND1, Reverse 5’ CCTCCTTCTGCACACATTTGAA 3’	This paper	NA
ASCL2, Forward 5’ CGCCTACTCGTCGGACGACAG 3’	This paper	NA
ASCL2, Reverse 5’ GCCGCTCGCTCGGCTTCCG 3’	This paper	NA
LGR5, Forward 5’ CTCTTCCTCAAACCGTCTGC 3’	This paper	NA
LGR5, Reverse 5’ GATCGGAGGCTAAGCAACTG 3’	This paper	NA
GAPDH, Forward 5’ GGAGTCAACGGATTTGGTCGTA 3’	This paper	NA
GAPDH, Reverse 5’ GGCAACAATATCCACTTTACCAGAGT 3’	This paper	NA